Effect of Fixation and Embedding on Raman Spectroscopic Analysis of Bone Tissue

Y. N. Yeni,[1] J. Yerramshetty,[2] O. Akkus,[3] C. Pechey,[1] C. M. Les[1]

[1]Bone and Joint Center, Henry Ford Hospital, 2799 West Grand Boulevard, Detroit, MI, USA
[2]Department of Bioengineering, University of Toledo, 2801 W. Bancroft Street, Toledo, OH, USA
[3]Weldon School of Biomedical Engineering, Purdue University, 500 Central Drive, West Lafayette, IN, USA

Abstract. Raman spectroscopy provides valuable information on the physicochemical properties of hard tissues. While the technique can analyze tissues in their native state, analysis of fixed, embedded, and sectioned specimens may be necessary on certain occasions. The information on the effects of fixatives and embedding media on Raman spectral properties is limited. We examined the effect of ethanol and glycerol as fixatives and a variety of embedding media (Araldite, Eponate, Technovit, glycol methacrylate, polymethyl methacrylate, and LR white) on Raman spectral properties (mineralization, crystallinity, and carbonation) measured from the cortical bone of mouse humeri. Humeri were fixed in ethanol or glycerol, followed by embedding in one of the media. Nonfixed, freeze-dried, and fixed but not embedded sections were also examined. Periosteal, endosteal, and midosteal regions of the intracortical envelope were analyzed. Raman spectra of fixative solutions and embedding media were also recorded separately in order to examine the specifics of overlap between spectra. We found significant effects of fixation, embedding, and anatomical location on Raman spectral properties. The interference of ethanol with tissue seemed to be relatively less pronounced than that of glycerol. However, there was no single combination of fixation and embedding that left Raman spectral parameters unaltered. We conclude that careful selection of a fixation and embedding combination should be made based on the parameter of interest and the type of tissue. It may be necessary to process multiple samples from the tissue, each using a combination appropriate for the Raman parameter in question.

Key words: Ethanol fixation — Glycerol fixation — Embedding medium — Raman spectroscopy — Cortical bone

Infrared (IR) and Raman spectroscopy are widely used to asses the composition and the physicochemical status of mineral and collagen phases of bone tissue [1–6]. IR spectroscopy generally operates in the transmittance mode, necessitating embedding and thin sectioning of the mineralized tissue. On the other hand, it is not essential to obtain thin sections for Raman analysis as it works in the reflectance mode. Even though the Raman analysis itself does not require thin sections, exposure of the inner volume of small or delicate samples may require embedding of the sample [5]. For instance, in our studies with zebrafish (*Danio rerio*) skeleton, we found it necessary to embed specimens in order to access the transverse sections of vertebrae, which have submillimetric dimensions. However, we were concerned that the embedding process may alter the composition and the physicochemical status of bone tissue, resulting in alterations in the spectral parameters such as mineralization, mineral crystallinity, and nonstoichiometric substitutions to mineral crystal lattice. These alterations may take place by way of different paths: (1) leaching of the mineral component to solutions utilized during fixation and embedding, (2) modifications in the vibrations of collagen bonds through alteration of their chemical environment, (3) overlap of the embedding medium-related peaks with bone-related peaks, which may confound the calculation of intensity ratios.

In their meticulous study, Aparicio et al. [7] systematically investigated the effects of various fixation and embedding processes on the IR spectral parameters of bone and determined those which had the least effect on the IR-detectable spectral parameters. While significant insight into the effect of fixation and embedding on the physicochemical properties of bone was provided, the optimal embedding sequence proposed for IR spectroscopic analysis of embedded bone tissue may not be optimal for Raman spectroscopic analysis of embedded bone. This assertion stems from the inherent differences between Raman and IR spectral analyses. In principle, nonpolar groups have strong Raman vibrations and polar groups generate stronger IR signals [8]. Therefore, peaks which are expressed strongly in IR spectroscopy would be expected to be weak in Raman and *vice versa*, resulting in differences between the interference patterns of embedding medium to mineral and collagen peaks in

---

Correspondence to: Y. N. Yeni; E-mail: yeni@bjc.hfh.edu

IR and Raman. For example, a bone-related band which is free from overlap of the embedding band in IR may not be immune from such interference in Raman due to emergence of other vibrational bands. Therefore, the optimal embedding medium for bone in IR spectroscopy may not necessarily be suitable in Raman mode. In this study, we sought to examine the effects of different fixation and embedding media on the mineralization, crystallinity, and type B carbonate substitution of bone tissue as derived by Raman spectroscopy.

Methods

Carcasses of littermate male Swiss-Webster mice were obtained from NAMSA Laboratories (Northwood, OH) immediately after their death via CO_2 hypoxia at the age of 9 weeks. These animals served as controls in another study under the approval of Institutional Animal Care and Use Committee (IACUC), and they did not receive medication or surgical intervention. Humeri were dissected and pooled in two separate groups as right and left humeri. Each experimental group consisted of either three left or three right humeri randomly selected from these groups so as to ensure that tissue from three different mice was present in each group. Thirty-six humeri were fixed in either 70% ethanol ($n = 18$) or glycerol ($n = 18$). Fixed samples were then embedded in one of six different media (Epon, LR white, glycol methacrylate [GMA], polymethyl methacrylate [PMMA], Technovit, and Araldite; $n = 3$ in each group). In order to isolate the effect of fixation in the whole process, six additional humeri were fixed in either ethanol or glycerol ($n = 3$ for each) without embedding. Three more humeri that were not fixed or embedded served as controls. After baseline measurements, the control group specimens were freeze-dried (Freeze Dryer 3; Labconco, Kansas City, MO) for 12 hours to remove unbound water without the confounding effects of chemical fixatives and measurements were repeated.

For specimens that would be embedded, all preliminary processing took place at room temperature, on a shaker table. Solution volumes were maintained at solution:specimen ratios of at least 10:1. No vacuum was used. Specimens fixed in glycerol were placed in 50% ethanol for 1 hour, followed by 70% ethanol for 1 hour. All specimens (glycerol- and ethanol-fixed) were then brought through an ascending ethanol series (70%, 90%, and three changes of 100% 1 hour apiece) before final processing and embedding.

Epon was from the Eponate 12 kit (catalog 18010; Ted Pella, Redding, CA). A mixture was made of 25.7 mL Eponate 12 resin, 9.3 mL dodecenyl succinic anhydride, 16.5 mL nadic methyl anhydride, and 0.8 mL 2,4,6-tri(dimethylaminomethyl)phenol. Specimens were infiltrated with a 50:50 mixture of this preparation and ethanol overnight. This was replaced with the preparation alone and polymerized at 60°C for 24 hours in glass molds. Glass molds were broken to release the finished blocks.

LR white was from an LR white kit (catalog 18181, Ted Pella). Specimens were infiltrated in a 50:50 mixture of 100% ethanol and LR white resin overnight and then in two changes of 100% LR white resin at 1 hour apiece. The specimens were then placed in glass molds, 10 cm under an 8 W 365 nm ultraviolet (UV) light (Spectroline EN180; Spectronics, Westbury, NY) for 24 hours. Glass molds were broken to release the finished blocks.

GMA was from a glycol methacrylate kit (catalog 18350, Ted Pella). Specimens were infiltrated for 15 minutes in a mixture of 80% GMA monomer and 20% distilled water, followed by 4 × 15-minute changes in 100% GMA. The final infiltration mixture was created by mixing seven parts 97% GMA/3% distilled water by volume with three parts 98% butyl methacrylate, 2% benzoyl peroxide paste by volume in an

Ehrlenmeyer flask and heating over a Bunsen burner under a fume hood until boiling (approximately 1−2 min). The flask was then plunged into an ice water bath until the mixture was cooled to 2°C. Specimens were infiltrated with two 1-hour changes of this mixture at room temperature, and the final infiltration and embedding took place overnight in the same mixture in glass molds, 10 cm under an 8 W 365 nm UV light. Glass molds were broken to release the finished blocks.

Technovit 7200VLC (Exakt, Oklahoma City, OK) specimens were infiltrated in two changes of a 50:50 mix of ethanol and Technovit 7200 resin, then two changes of 100% Technovit 7200 resin. Final embedding took place in plastic molds in 100% Technovit 7200 resin in a water-cooled, light-embedding module (Light Fixture Type 43, yellow light 9W/41-827, blue light 9W/91; Exakt), with 3 hours under yellow light, followed by 10 hours under blue light. The blocks were then removed from the plastic molds.

PMMA (methyl methacrylate [MMA] monomer, catalog 03629-4; Fisher, Fair Lawn, NJ) specimens were brought through three 1-hour changes of xylene, followed by two 1-hour changes of MMA monomer. Final infiltration and polymerization took place in glass molds, using a mixture of 5 g benzoyl peroxide (97%, catalog 179981-500 g; Sigma-Aldrich, Milwaukee, WI) per liter of MMA monomer in a 37°C water bath until polymerized (approximately 7 days). Glass molds were broken to release the finished blocks.

Araldite was from the Araldite 502 kit (catalog 18050, Ted Pella). Mixtures were prepared according to the procedure of Luft [9]. Components were warmed to 60°C before mixing. Araldite 502 (27 mL) was mixed with 23 mL dodecenyl succinic anhydride and 0.75 mL 2,4,6-tri(dimethylaminomethyl)phenol. Specimens were infiltrated with a 50:50 mixture of this preparation and ethanol overnight. This was replaced with the preparation alone and polymerized at 60°C for 24 hours in glass molds. Glass molds were broken to release the finished blocks.

Humeri were sectioned in a plane perpendicular to the longitudinal axis of the mid-diaphyseal shaft using a cutting-grinding system (Exakt). The surface was hand-ground and polished, with the final polish being accomplished with 0.05 μm polishing suspension (Masterprep Polishing Suspension, catalog 40-6377-032; Buehler, Lake Bluff, IL). Raman analysis was performed along the exposed transverse section, within the cortical thickness of the medial quadrants of humeri. Raman spectral analysis was limited to the medial quadrant at the mid-diaphysis so as to minimize the effects of anatomical variations in composition of bone between quadrants and along the longer axis. Raman spectra of polymerized embedding media were also recorded in order to gain insight into the overlapping between the Raman peaks of each medium and bone tissue.

A Raman microscope (LabRam; Horiba Jobin Yvon, Edison, NJ) was used to assess the mineralization, crystallinity, and carbonate substitution of bone tissue. The Raman system consists of a 633 nm He-Ne laser source, a microscope (BX41; Olympus, Tokyo, Japan), and a charge-coupled device detector coupled to a stigmatic spectrometer. The instrument has an automated x-y mapping stage that enables capture of an array of spectra over a defined region. A microscope objective transmits the laser light excitation and collects the reflected photons, which are relayed to the spectrometer and separated based on their wavenumber. The compositional and physicochemical information of the illuminated spot is then extracted from this wavenumber spectrum.

Nine spectra were recorded, three of which were close to the endosteal envelope (about 125 μm), three at the mid-cortical thickness, and three close to the periosteal envelope (about 125 μm). Measurement points were spaced about 100 μm from each other. Spectra were recorded within the wavenumber range of 800−1,750 cm^{-1}, which covers the signature bands of mineral and collagen phases. Each scan was repeated three times at the same area of interest, and the resulting spectrum from each point was the average of these three consecutive scans, each 45 seconds long. The resulting wavenumber resolution of spectra was 1 cm^{-1}.

The data were acquired using LabSpec software (Horiba Jobin Yvon) and analyzed using a custom-written MATLAB code (Mathworks, Natick, MA). The code filters the data using a three-point linear moving average and generates a template baseline, which is then used to subtract the background fluorescence from the spectrum. Required band intensities are obtained by calculating the peak intensity with respect to a local baseline. Mineralization was calculated in two ways: (1) PO_4^{3-}/CH_2 ratio, the ratio of the phosphate symmetric-stretch band intensity (at 960 cm^{-1}) to the intensity of vibrations resulting from the CH_2 side-chains of collagen molecules (at 1,450 cm^{-1}), and (2) $PO_4^{3-}/$amide I ratio, the ratio of the phosphate symmetric-stretch band intensity (at 960 cm^{-1}) to amide I resulting from the backbone vibrations of the collagen (at 1,667 cm^{-1}). In the case of fresh unembedded bone tissue, the mineralization values obtained from the two bands are correlated and using one over the other does not pose a distinct advantage in terms of assessing mineralization.

However, fixation-induced dehydration and the overlap of embedding medium-related peaks may differ between the two bands. Therefore, both bands were considered to allow identification of the band affected the least from the overlap of fixation and embedding-related vibrations. An increasing mineralization ratio indicates a more mineralized collagen matrix. Type B carbonate content substitution (carbonate ions which substitute for phosphate positions) was calculated as the ratio between the intensities of phosphate symmetric-stretch band and the respective peak of type B carbonate symmetric-stretch band (at 1,068 cm^{-1}) [10, 11]. Crystallinity was calculated as the inverse of the width of the phosphate symmetric-stretch band at half the maximum intensity value [12].

For statistical analyses, mixed model procedures of SPSS (SPSS, Chicago, IL) were employed. *Post hoc* analysis of significant results was performed using Fisher's least significant difference test. First, the effect of fixatives was examined using the groups that were not subjected to fixative solutions and those that were subjected to fixatives but not embedded. Each bone was introduced in the statistical model as a subject variable, fixative and anatomical location were fixed effects, while each Raman parameter was the dependent variable. In order to account for the fact that multiple locations from each bone were examined, anatomical location (periosteum, midosteum, and endosteum) was introduced as a repeated effect.

In order to examine whether embedding in a medium further affected the Raman parameters, all embedded groups were compared to their respective fixed-but-not-embedded controls. In these analyses, each bone was introduced in the model as a subject variable, embedding medium and anatomical location were fixed effects, with each Raman parameter as the dependent variable. Anatomical location was introduced as a repeated effect, and the group that was fixed but not embedded was represented with an embedding medium type of "none."

Comparison of normal and freeze-dried measurements was done using a two-way repeated measures analysis of variance with bone as a subject variable and anatomical location and treatment (normal vs. freeze-dried) as factors.

Results

Comparison of Fixatives

Comparison of nonembedded control, ethanol-fixed, and glycerol-fixed bones revealed that fixation had a significant effect on mineralization (both from amide I and CH_2wag) ($P < 0.001$) and crystallinity ($P < 0.008$) (Tables 1, 2, 4). Fixation did not affect the carbonation (Tables 3 and 4) and within-specimen scatter of crystallinity and mineralization ($0.09 < P < 0.77$). Glycerol-fixed bones had a significantly greater $PO_4^{3-}/$AmideI ratio,

a lower PO_4^{3-}/CH_2 ratio, and less crystallinity than controls ($P < 0.001$, $P < 0.001$, and $P = 0.032$, respectively), whereas differences between ethanol-fixed and control specimens were marginally significant for the PO_4^{3-}/CH_2 ratio and crystallinity ($P = 0.095$ and $P = 0.084$, respectively) but the $PO_4^{3-}/$AmideI ratio in ethanol-fixed specimens was greater than in controls ($P < 0.001$). Overall, both fixatives affected the mineral-to-matrix ratios, with ethanol's effect being less pronounced.

A marginally significant effect of anatomical location on both the PO_4^{3-}/CH_2 and $PO_4^{3-}/$AmideI ratios was found ($P = 0.059$ and $P = 0.051$, respectively), but these differences did not depend on the fixative type ($P > 0.13$ for interaction of fixative and anatomical location), indicating that effects of fixation were similar across the cortical thickness. No other significant effect of anatomical location was found for carbonation and crystallinity between control, ethanol-fixed, and glycerol-fixed specimens ($0.24 < P < 0.99$).

None of the Raman parameters differed between freeze-dried bones and wet controls, with the only exception of an increase in $PO_4^{3-}/$Amide I in freeze-dried bone ($P < 0.002$).

Comparison of Embedding Media with Reference to Corresponding Fixative

Ethanol-fixed specimens. When each ethanol-fixed embedded group was compared to its own ethanol-fixed control (specimens fixed in ethanol but not embedded), it was found that embedding had a significant effect on the mean as well as on the scatter of the PO_4^{3-}/CH_2 ratio ($P = 0.013$ and $P < 0.001$, respectively) but that of the $PO_4^{3-}/$AmideI ratio was not affected significantly ($P > 0.16$ for both). Embedding also affected crystallinity ($P = 0.004$) and carbonation ($P < 0.001$). No significant effect of embedding was found for the scatter of crystallinity ($P > 0.48$) or for the scatter of carbonation ($P > 0.94$).

The difference in PO_4^{3-}/CH_2 ratio between ethanol-fixed and ethanol-fixed araldite-embedded specimens was not significant ($P = 0.105$), whereas all other embedding media resulted in significantly different PO_4^{3-}/CH_2 values compared to ethanol-fixed specimens ($0.001 < P < 0.037$). The scatter of PO_4^{3-}/CH_2, on the other hand, was significantly different from ethanol-only specimens for all embedding media ($0.001 < P < 0.033$) but Epon ($P = 0.197$). The difference in crystallinity between ethanol-fixed and GMA-embedded specimens was not significant ($P = 0.303$), whereas all other embedding media resulted in significantly different crystallinity values compared to ethanol-only specimens ($0.001 < P < 0.028$). The carbonation of specimens embedded in GMA, LR white, or PMMA did not differ from ethanol-only specimens ($0.20 < P < 0.75$), whereas all other embedding media resulted in signifi-

Table 1a. Average mineralization calculated from the CH_2-wag peak (Mean ± SD)

	None				Ethanol				Glycerol			
	PO	MO	EO	Pool	PO	MO	EO	Pool	PO	MO	EO	Pool
None	12.91 ± 4.08	12.16 ± 2.30	11.04 ± 2.06	12.04 ± 2.94	11.19 ± 2.04	9.40 ± 3.19	10.04 ± 2.56	10.16 ± 2.62	5.19 ± 1.22	5.53 ± 1.16	4.36 ± 1.49	5.13 ± 1.34
Epon					6.97 ± 2.14	7.67 ± 2.40	8.44 ± 2.20	7.69 ± 2.24	7.78 ± 1.33	7.67 ± 2.17	9.23 ± 2.20	8.23 ± 2.00
Araldite					7.60 ± 2.24	8.86 ± 2.04	8.84 ± 2.35	8.34 ± 2.16	9.93 ± 1.48	9.08 ± 1.33	8.89 ± 1.96	9.31 ± 1.61
LR Wh					6.19 ± 0.98	6.67 ± 1.12	5.94 ± 1.49	6.26 ± 1.21	7.07 ± 0.79	7.38 ± 0.78	6.10 ± 2.41	6.85 ± 1.57
PMMA					5.69 ± 0.49	5.01 ± 0.77	5.21 ± 0.56	5.31 ± 0.66	5.26 ± 0.86	6.93 ± 2.52	6.89 ± 2.47	6.35 ± 2.16
Techno					8.25 ± 2.28	6.75 ± 1.41	7.25 ± 1.30	7.42 ± 1.77	7.10 ± 1.26	8.05 ± 0.86	7.48 ± 1.37	7.54 ± 1.20
GMA					6.28 ± 0.83	6.17 ± 1.26	6.57 ± 1.36	6.34 ± 1.12	6.15 ± 0.73	5.96 ± 1.47	5.57 ± 1.30	5.89 ± 1.19

Table 1b. Average mineralization calculated from the amide I peak (Mean ± SD)

	None				Ethanol				Glycerol			
	PO	MO	EO	Pool	PO	MO	EO	Pool	PO	MO	EO	Pool
None	6.49 ± 2.11	6.95 ± 1.98	6.26 ± 1.62	6.57 ± 1.86	9.14 ± 1.58	7.46 ± 1.36	8.70 ± 1.05	8.43 ± 1.48	8.04 ± 1.26	7.76 ± 1.96	7.20 ± 2.36	7.67 ± 1.87
Epon					7.51 ± 2.16	7.49 ± 2.40	7.75 ± 1.69	7.58 ± 2.02	7.60 ± 1.10	7.68 ± 2.55	8.62 ± 2.80	7.97 ± 2.24
Araldite					6.79 ± 1.71	6.16 ± 1.45	7.56 ± 1.89	6.84 ± 1.74	7.90 ± 1.76	8.31 ± 2.09	8.41 ± 1.18	8.21 ± 1.66
LR Wh					10.84 ± 2.98	8.63 ± 3.16	8.14 ± 2.00	9.20 ± 4.41	7.96 ± 0.52	7.40 ± 0.77	6.66 ± 1.89	7.34 ± 1.29
PMMA					8.83 ± 1.55	8.60 ± 1.91	7.20 ± 1.62	8.21 ± 1.79	10.07 ± 3.20	10.50 ± 2.47	10.44 ± 3.15	10.34 ± 3.37
Techno					11.69 ± 2.64	10.66 ± 2.40	10.40 ± 1.52	10.91 ± 2.22	8.14 ± 3.37	8.36 ± 2.00	9.01 ± 2.54	8.50 ± 2.61
GMA					8.77 ± 2.52	10.45 ± 1.83	11.88 ± 3.75	10.37 ± 2.95	8.93 ± 2.94	7.62 ± 2.57	7.38 ± 2.61	7.98 ± 2.70

PO, MO and EO represent periosteal, mid-osteal and endosteal regions, respectively; SD, standard deviation

cantly different carbonation values compared to ethanol-fixed specimens ($0.001 < P < 0.037$).

A significant effect of anatomical location on crystallinity and carbonation was found for the ethanol-fixed group ($P < 0.012$). It was the periosteal region that was different from others for both parameters ($P < 0.01$). While there was no significant interaction between anatomical location and embedding medium for crystallinity ($P > 0.41$), a significant interaction was found between the two ($P < 0.039$) for carbonation. These interactions indicate that the effect of embedding medium on crystallinity does not depend on cortical region, whereas the effect of embedding on carbonation measurements depends on which cortical region is examined.

Glycerol-fixed specimens. When each glycerol-fixed embedded group was compared with the glycerol-fixed group, a significant effect of embedding on the average PO_4^{3-}/CH_2 ratio ($P < 0.001$) and average carbonation ($P = 0.018$) was found. The effect of embedding on other parameters was not significant ($0.10 < P < 0.57$).

The PO_4^{3-}/CH_2 ratio in specimens embedded in GMA and PMMA was not significantly different from that for specimens fixed in glycerol ($P = 0.383$ and $P = 0.113$, respectively), whereas all other embedding media resulted in significantly different PO_4^{3-}/CH_2 ratios compared to the glycerol-fixed group ($0.001 < P < 0.024$). While specimens embedded in Araldite had carbonation values significantly different ($P < 0.001$) from glycerol-fixed specimens, those embedded in other media were not significantly different ($0.15 < P < 0.79$ for all except Technovit, which had a marginal P value of 0.065).

Anatomical location had a significant effect on average crystallinity ($P = 0.003$) and within-specimen scatter of PO_4^{3-}/CH_2 ratio ($P = 0.015$) and $PO_4^{3-}/$ AmideI ratio ($P = 0.006$). There was also a marginal

Table 2. Average crystallinity calculated from the phosphate peak (mean ± SD)

	None				Ethanol				Glycerol			
	PO	MO	EO	Pool	PO	MO	EO	Pool	PO	MO	EO	Pool
None	0.0517± 0.0027	0.0517± 0.0009	0.0514± 0.0012	0.0516± 0.0017	0.0501± 0.0012	0.0483± 0.0025	0.0506± 0.0011	0.0497± 0.0019	0.0528± 0.0023	0.0535± 0.0031	0.0525± 0.0022	0.0530± 0.0033
Epon					0.0536± 0.0027	0.0521± 0.0017	0.0515± 0.0016	0.0524± 0.0022	0.0535± 0.0021	0.0531± 0.0009	0.0524± 0.0015	0.0531± 0.0015
Araldite					0.0574± 0.0025	0.0529± 0.0030	0.0539± 0.0028	0.0548± 0.0035	0.0555± 0.0025	0.0554± 0.0019	0.0547± 0.0023	0.0551± 0.0023
LR white					0.0527± 0.0024	0.053± 0.0017	0.0505± 0.0021	0.0521± 0.0028	0.0535± 0.0016	0.0541± 0.0018	0.0512± 0.0032	0.0529± 0.0026
PMMA					0.0528± 0.0008	0.0513± 0.0010	0.0518± 0.0015	0.0520± 0.0021	0.0552± 0.0030	0.0527± 0.0013	0.0519± 0.0031	0.0533± 0.0029
Technovit					0.0543± 0.0035	0.0521± 0.0017	0.0521± 0.0019	0.0528± 0.0026	0.0545± 0.0014	0.0532± 0.0019	0.0528± 0.0009	0.0535± 0.0016
GMA					0.0509± 0.0003	0.0508± 0.0024	0.0507± 0.0004	0.0508± 0.0021	0.0521± 0.0011	0.0515± 0.0019	0.0523± 0.0014	0.0519± 0.0015

PO, MO, and EO represent periosteal, mid-osteal, and endosteal regions, respectively; SD, standard deviation

Table 3. Average carbonation (mean ± SD)

	None				Ethanol				Glycerol			
	PO	MO	EO	Pool	PO	MO	EO	Pool	PO	MO	EO	Pool
None	0.168± 0.041	0.158± 0.022	0.161± 0.011	0.162± 0.026	0.175± 0.017	0.203± 0.043	0.168± 0.030	0.181± 0.034	0.206± 0.102	0.173± 0.085	0.211± 0.101	0.196± 0.094
Epon					0.139± 0.023	0.141± 0.023	0.149± 0.022	0.143± 0.022	0.133± 0.022	0.136± 0.015	0.138± 0.022	0.135± 0.019
Araldite					0.039± 0.040	0.101± 0.039	0.111± 0.034	0.083± 0.043	0.085± 0.033	0.081± 0.026	0.098± 0.019	0.088± 0.026
LR white					0.167± 0.037	0.162± 0.025	0.188± 0.046	0.172± 0.037	0.151± 0.023	0.146± 0.028	0.177± 0.047	0.158± 0.036
PMMA					0.151± 0.041	0.163± 0.023	0.164± 0.019	0.159± 0.029	0.113± 0.044	0.165± 0.033	0.149± 0.029	0.142± 0.041
Technovit					0.115± 0.049	0.144± 0.021	0.151± 0.020	0.137± 0.035	0.101± 0.030	0.139± 0.027	0.141± 0.017	0.127± 0.031
GMA					0.183± 0.029	0.175± 0.050	0.167± 0.014	0.176± 0.033	0.161± 0.017	0.167± 0.022	0.152± 0.025	0.160± 0.023

PO, MO, and EO represent periosteal, mid-osteal, and endosteal regions, respectively; SD, standard deviation

effect on average carbonation ($P = 0.061$), with a tendency of carbonation to increase from periosteal to endosteal regions. No other significant effect was found ($0.28 < P < 0.89$ for other Raman parameters). All significant differences found in the above parameters were between the periosteal and endosteal cortices ($P < 0.004$), but these differences did not depend on which embedding medium was used ($0.08 < P < 0.239$).

There was a notable overlap between the Raman spectra of normal bone tissue and that fixed in glycerol or ethanol (Fig. 1a, b); however, the amide I region was mostly free from that interference. Ethanol also seemed to have a weak presence in the wavenumber range where carbonate peak is located ($\sim$1,071 cm^{-1}). Overlap between fresh bone tissue and embedding medium varied (Fig. 2a–f). All embedding media had a very strong

presence in the CH$_2$-wag region consistently. GMA, LR white, PMMA, and Technovit had some presence in the amide I range; however, their contribution at the wavenumber (1,667 cm^{-1}) used to calculate mineralization score was negligible. In the phosphate symmetric-stretch region, Epon and Araldite had a weak presence, LR white and Technovit had a moderate presence, and GMA and PMMA had a strong presence. PMMA and Araldite had weak contributions in the carbonate symmetric-stretch range.

Discussion

Aging, disease, and genetic disorders affect the makeup of bone's extracellular matrix directly or by way of altering the function of bone cell populations. Micro-

Table 4. Summary of the effects of fixation and embedding on Raman spectral parameters of cortical bone[a]

	Epon	Araldite	LR white	PMMA	Technovit	GMA
PO_4^{3-}/CH_2 ratio	↔↓/↓↑	↔↔/↓↑	↔↓/↓↑	↔↓/↓↔	↔↓/↓↑	↔↓/↓↔
$PO_4^{3-}/Amide I$ ratio	↑↔/↑↔	↑↔/↑↔	↑↔/↑↔	↑↔/↑↔	↑↔/↑↔	↑↔/↑↔
Crystallinity	↔↑/↓↔	↔↑/↓↔	↔↑/↓↔	↔↑/↓↔	↔↑/↓↔	↔↔/↓↔
Type B carbonation	↔↓/↔↔	↔↓/↔↓	↔↔/↔↔	↔↔/↔↔	↔↓/↔↔	↔↔/↔↔

[a] ↔, ↓, and ↑ indicate no change, decrease, and increase, respectively, in the parameter due to the effect (fixed in ethanol followed by embedding in medium/fixed in glycerol followed by embedding in medium). The best combination of fixation and embedding medium is set in bold for a given fixation-embedding sequence
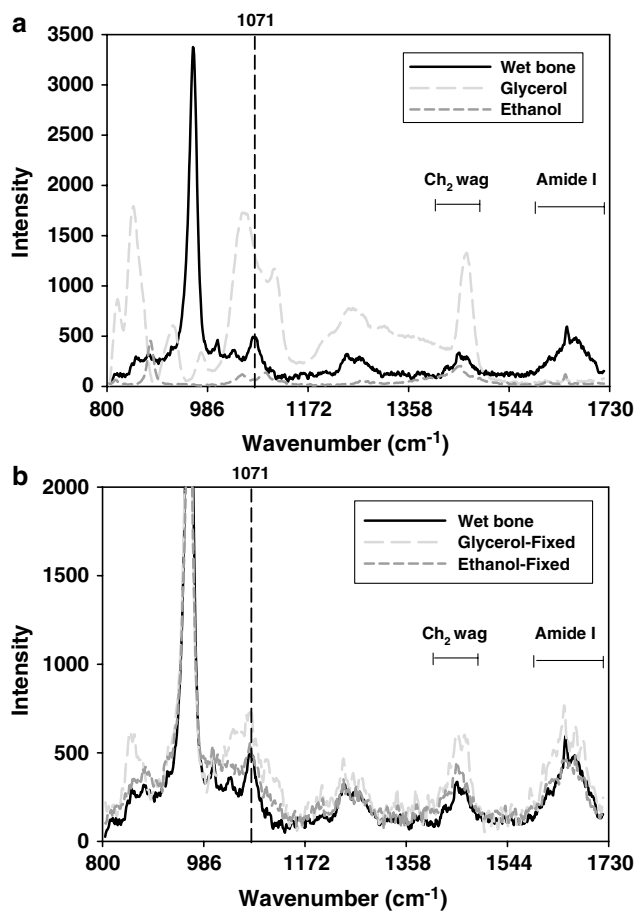

Fig. 1. (a) Raman spectrum of fixative solutions plotted with that of wet bone for demonstration of overlap between spectra. (b) Raman spectrum of normal bone, glycerol-fixed bone, and ethanol-fixed bone.

study, we investigated the effects of commonly used histological fixation and embedding processes on the bone matrix compositional variables as obtained by Raman spectral analysis. Overall, both fixation and embedding processes altered the spectral signature of bone tissue to an extent that the parameters derived from spectra were significantly different from fresh hydrated bone tissue.

Through replacement of water molecules, the fixation process essentially preserves cellular details and prepares the tissue for embedding. The replacement of tightly bound water molecules in the immediate vicinity of mineral and collagen molecules by fixatives is not possible [13]. On the other hand, removal of loosely bound and unbound water molecules interferes with the conformation of tightly bound water and affects the supramolecular packing pattern of collagen molecules. Removal of water by bench or oven drying is known to result in closer spacing of collagen matrix [14−16]. Any changes in the lateral spacing of collagen molecules and the bound water structure perturb the secondary structure of collagen and, resultingly, the peptide bond conformation. Therefore, the primary effect of fixation would be on the amide bands of the Raman spectral pattern, which are mostly composed of peptide vibrations [17]. The amide I band has an additional level of sensitivity to dehydration since there is a broad band of H_2O ν_2−bending vibrations centered at 1,645 cm^{-1} [18]. Dehydration removes this broad water band with an associated reduction in amide I intensity, which in turn results in an increase in the mineralization parameter calculated from amide I intensity. Attesting to this, the mineralization parameter calculated using the amide I peak increased in freeze-dried bone. The increase in the mineralization parameter calculated using the amide I peak after fixation in glycerol and ethanol (Table 2) is consistent with dehydration of the tissue through removal of free water by the fixative.

Unlike the backbone amide I vibrations, the CH_2 wag stems from side-chains; thus, it is less amenable to changes in the secondary conformation or other alterations in collagen structure. There are other sources of CH_2 intensity besides collagen; however, this is true also for the other two bands emanating from backbone amide vibrations. Therefore, the latter do not serve as
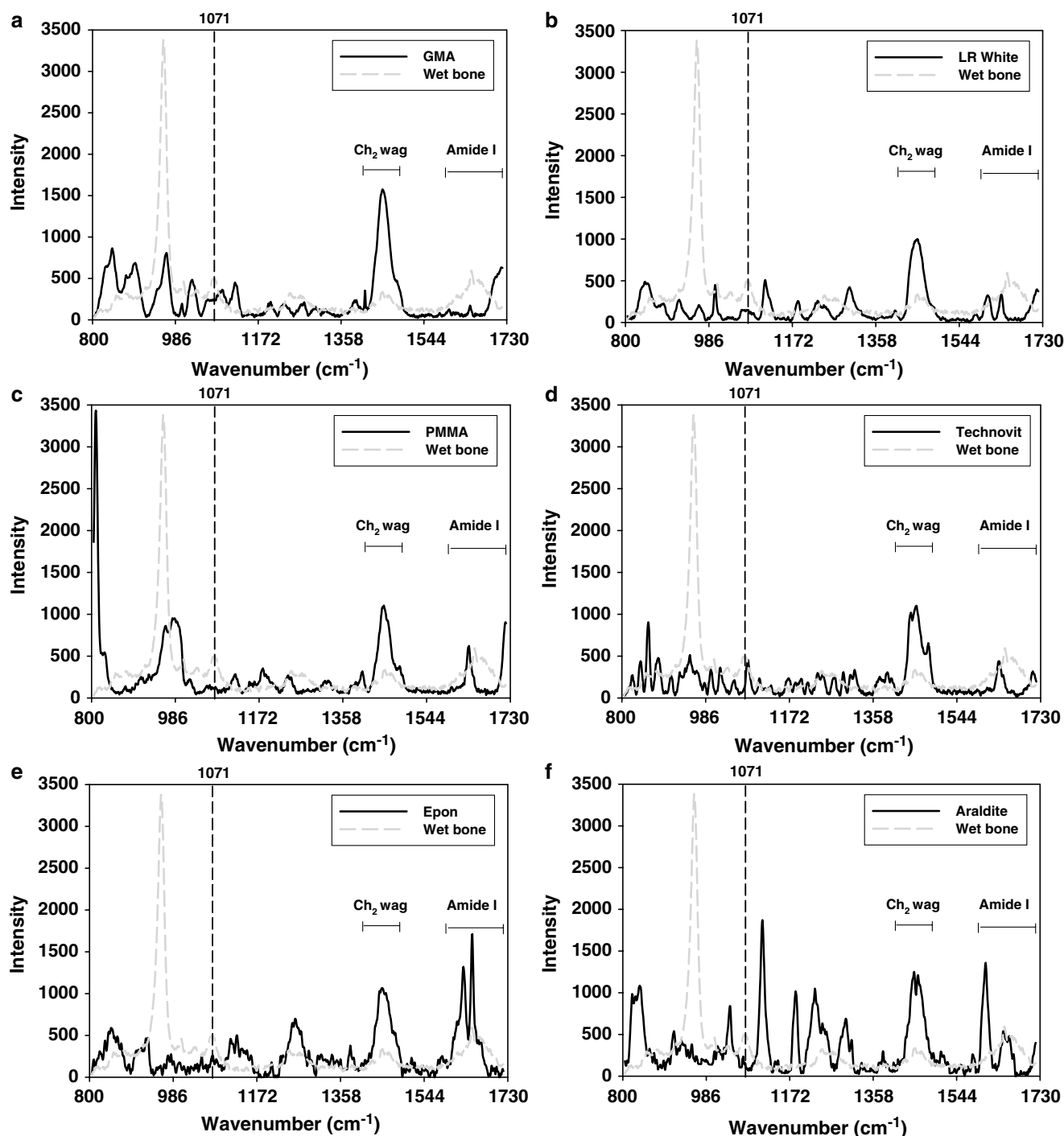
spectroscopy adds a spatial dimension to the assessment of bone matrix quality during these disorders at the order of micrometers. This level of dimensional resolution becomes particularly essential when small animal models such as mice or zebrafish are utilized for the investigation. Skeletal organs of such animals are very small, making it necessary to embed them so as to expose bone matrix in a controlled and repeatable manner. Therefore, it becomes of utmost importance to identify the effects of tissue processing on the compositional parameters obtained from spectral analysis. In this

Fig. 2. Raman spectrum of embedding media plotted with that of wet bone for demonstration of overlap between spectra. (**a**) GMA, (**b**) LR white, (**c**) PMMA, (**d**) Technovit, (**e**) Epon, (**f**) Araldite.

better alternatives to the CH_2 band. It is reasonable to assume that CH_2 band intensity is a correlate of the collagen content in the current setting due to the abundance of collagen in bone and limited expected variation of noncollagenous sources in these littermate mice. With these in mind, for ethanol fixation, the changes in the mineralization score calculated using CH_2 intensity were minimal (borderline significant,

$P = 0.09$). This minimal effect was likely due to rapid evaporation of the ethanol from the surface of the sample where spectra were captured; therefore, the overlap of ethanol-related peaks with bone's spectral signature was not a concern. Unlike ethanol, glycerol stayed within bone matrix and had a strong peak which coincided with the CH_2 band of bone (Fig. 1a). Therefore, the intensity of CH_2 vibrations increased following

glycerol fixation (Fig. 1b), resulting in reduction of the mineralization parameter calculated using CH_2 intensity (Table 1a). Therefore, as CH_2 is the least sensitive band to dehydration, we recommend using the fixation medium which affects it the least, ethanol in the current case.

The effects of embedding medium on Raman spectrum of bone tissue may occur by band overlap and/or by interaction of chemical groups between bone matrix and embedding medium. The latter has been ruled out at least for PMMA by Pleshko et al. [19]; however, other embedding media may induce shifts in the wavenumbers of mineral or collagen bands. For moderately to highly mineralized tissue, the diffusion of embedding media is limited [19] due to lack of void space and high packing density in mineralized collagen matrix [15, 16]. In the current study, the anatomical location selected was mineralized; therefore, we did not observe a gross appearance of plastic peaks in spectra of embedded bone tissue. Only one specimen in the Araldite-embedded group displayed a noticeable emergence of Araldite peaks in three out of nine observations. Yet, diffusion of embedding media is expected to occur to a certain extent and the overlap of embedding media peaks with those of bone tissue is a concern (Fig. 2). Unfortunately, the CH_2 band, which is affected the least by fixation, is affected the most by embedding medium. With the exceptions of Epon and Araldite, the portion of the amide I range (at $1,667 \text{ cm}^{-1}$) which was utilized for calculation of mineralization was not confounded by the bands of embedding media. Therefore, the amide I range seems to be the least affected by overlap effects; however, unfortunately, it is highly susceptible to dehydration induced during fixation.

For ethanol-fixed samples there was an overall increase in crystallinity after embedding, with Araldite having the most pronounced effect. This effect could be due to overlap of embedding peaks for GMA, PMMA, and Technovit as they have a strong presence in the phosphate range. However, LR white, Epon, and particularly Araldite increased the crystallinity despite their weak presence in this range. Crystallinity is affected by changes in the stoichiometry or size and shape of mineral crystals. Increasing crystallinity indicates a more ordered lattice structure (fewer substitutions), a greater crystal, or changes in the strain environment of the lattice. For Araldite, it was also observed that the carbonate-to-phosphate ratios were significantly lowered following embedding. The reduction in this ratio agrees with the increase in crystallinity as well [1]. It appears as if carbonate may have an affinity to dissolve in Araldite. Alternatively, the pH of the embedding medium may be relatively more acidic, resulting in dissolution of poorly crystalline mineral at a greater rate than the more crystalline counterpart. Thereby, the overall crystallinity may have increased due to this selective dissolution of imperfect crystallites. We used standardized methods for embedding; however, we did not measure the pH of

media during the experiment. One final possibility that may have led to increased crystallinity could be the recrystallization of dissolved crystallites. Further validation of these assertions via direct quantification of crystallite dimensions using techniques such as X-ray diffraction would be valuable.

One approach to counteract the overlap effects of embedding would be subtraction of the embedding background (so-called Raman difference spectrum analysis). Subtraction requires a peak in the embedding medium which occurs at a location where the bone spectrum has no bands so that it could be used as a hallmark to scale a model embedding spectrum that will be subtracted from the embedded bone spectrum. In the wavenumber range we covered, it was not possible to identify such a band for any medium. However, lower or higher wavenumbers may reveal such a peak for different media. Another complication working against subtraction is the dependence of penetration on the extent of mineralization. Different levels of mineralization will result in different levels of embedding perfusion over space, making a simple subtraction process a difficult task. For IR analysis, similar hardships in applicability of subtraction methods are discussed in detail by Aparicio et al. [7]. Another approach to the elimination of embedding peaks would be principal component analysis. Recently, Morris et al. [20] demonstrated that it is possible to identify the presence of embedding medium using principal component analysis. While they identified the presence of medium, they did not attempt to eliminate it. Using the score of the medium at a given location as a scaling factor, one may be able to subtract out the embedding medium. The use of principal component analysis for this purpose requires further investigation.

It is clear that the processing of bone tissue without altering bone's composition is not a trivial issue. These results demonstrate that no unique processing method will preserve the original composition as assessed via Raman parameters, similar to the conclusion for IR parameters [7]. However, careful selection of a few fixation/embedding combinations could allow measurement of much of the compositional details (Table 4). The results show that ethanol fixation will be relatively favorable compared to glycerol fixation. Following ethanol fixation, embedding two comparable samples, one in Araldite and the other in GMA, appears to capture all major Raman parameters but the $PO_4^{3-}/$ AmideI ratio. If the scatter of physiochemical parameters within a bone is of interest, one might add embedding in Eponate to the list. The interactions of anatomical location and embedding procedures are probably due to the differences in the perfusion characteristics of regions. The extent to which tissue properties will be affected by processing may depend on the bone source, and it may be necessary to evaluate these effects for the specific tissue under question.

Finally, a comparison of Raman measurements with different techniques such as Fourier transform IR, X-ray diffraction, and chemical analysis would be helpful for more accurate interpretation of current findings and for taking better advantage of these complementary methods.

References

1. Rey C, Collins B, Goehl T, Dickson IR, Glimcher MJ (1989) The carbonate environment in bone mineral: a resolution-enhanced Fourier transform infrared spectroscopy study. Calcif Tissue Int 45:157−164
2. Paschalis EP, Jacenko O, Olsen B, Mendelsohn R, Boskey AL (1996) Fourier transform infrared microspectroscopic analysis identifies alterations in mineral properties in bones from mice transgenic for type X collagen. Bone 19:151−156
3. Grynpas MD, Rey C (1992) The effect of fluoride treatment on bone mineral crystals in the rat. Bone 13:423−429
4. Casciani FS, Etz ES, Newbury DE, Doty SB (1979) Raman microprobe studies of two mineralizing tissues: enamel of the rat incisor and the embryonic chick tibia. Scan Electron Microsc 2:383−391
5. Timlin JA, Carden A, Morris MD, Rajachar RM, Kohn DH (2000) Raman spectroscopic imaging markers for fatigue-related microdamage in bovine bone. Anal Chem 72:2229−2236
6. Akkus O, Polyakova-Akkus A, Adar F, Schaffler MB (2003) Aging of microstructural compartments in human compact bone. J Bone Miner Res 18:1012−1019
7. Aparicio S, Doty SB, Camacho NP, Paschalis EP, Spevak L, Mendelsohn R, Boskey AL (2002) Optimal methods for processing mineralized tissues for fourier transform infrared microspectroscopy. Calcif Tissue Int 70:422−429
8. Wilson EB, Cross PC, Decius JC (1980) Molecular Vibrations: The Theory of Infrared and Raman Vibrational Spectra. Dover Publications, New York, NY
9. Luft JH (1961) Improvements in epoxy resin embedding methods. J Biophys Biochem Cytol 9:409−414
10. Frushour BG, Koenig JL (1975) Raman scattering of collagen, gelatin, and elastin. Biopolymers 14:379−391
11. Penel G, Leroy G, Rey C, Bres E (1998) MicroRaman spectral study of the PO_4 and CO_3 vibrational modes in synthetic and biological apatites. Calcif Tissue Int 63:475−481
12. Freeman JJ, Wopenka B, Silva MJ, Pasteris JD (2001) Raman spectroscopic detection of changes in bioapatite in mouse femora as a function of age and in vitro fluoride treatment. Calcif Tissue Int 68:156−162
13. Bachmann L, Gomes ASL, Zezell DM (2004) Bound energy of water in hard dental tissues. Spectrosc Lett 37:565−579
14. Finlay JB, Hardie WR (1994) Anisotropic contraction of cortical bone caused by dehydration of samples of the bovine femur in vitro. Proc Inst Mech Eng [H] 208:27−32
15. Lees S, Heeley JD, Cleary PF (1981) Some properties of the organic matrix of a bovine cortical bone sample in various media. Calcif Tissue Int 33:83−86
16. Lees S (1981) A mixed packing model for bone collagen. Calcif Tissue Int 33:591−602
17. Doyle BB, Bendit EG, Blout ER (1975) Infrared spectroscopy of collagen and collagen-like polypeptides. Biopolymers 14:937−957
18. Starzak M, Mathlouthi M (2003) Cluster composition of liquid water derived from laser-Raman spectra and molecular simulation data. Food Chem 82:3−22
19. Pleshko NL, Boskey AL, Mendelsohn R (1992) An FT-IR microscopic investigation of the effects of tissue preservation on bone. Calcif Tissue Int 51:72−77
20. Morris MD, Crane NJ, Gomez LE, Ignelzi MA Jr (2004) Compatibility of staining protocols for bone tissue with Raman imaging. Calcif Tissue Int 74:86−94